Multidisciplinary Cancer Investigation Original Article

January 2023, Volume 7, Issue 1

Discriminating Malignant and Benign Brain Tumors Using Texture Features of MRI-ADC Images

Sahan M. Vijithananda[1], Mohan L. Jayatilake[2,*], Teresa C. Gonçalves[3], Luis M. Rato[3], Bimali S. Weerakoon[2], Tharindu D. Kalupahana[4], Anil De Silva[5], Karuna Dissanayake[6], Padma B. Hewavithana[1]

[1] Department of Radiology, Faculty of Medicine, University of Peradeniya, Peradeniya, Sri Lanka
[2] Department of Radiography/Radiotherapy, Faculty of Allied Health Sciences, University of Peradeniya, Peradeniya, Sri Lanka
[3] Department of Informatics, School of Science and Technology, University of Evora, Evora, Portugal
[4] Department of Computer Engineering, Faculty of Engineering, University of Sri Jayewardenepura, Ratmalana, Sri Lanka
[5] Department of Radiology, National Hospital of Sri Lanka, Colombo, Sri Lanka
[6] Department of Histopathology, National Hospital of Sri Lanka, Colombo, Sri Lanka
**Corresponding author: Mohan L. Jayatilake, Department of Radiography/Radiotherapy, Faculty of Allied Health Sciences, University of Peradeniya, Peradeniya, Sri Lanka. Tel: +94770195222; Fax: +94812387394; E-mail: jayatiml@pdn.ac.lk*

DOI: 10.30699/mci.7.1.630-1

Submitted: 16 January 2023
Revised: 01 March 2023
Accepted: 03 March 2023
e-Published: 25 March 2023

Keywords:
Magnetic Resonance Imaging
Malignant Brain Neoplasm
Benign Brain Neoplasm
Diffusion Weighted MRI

Introduction: The diagnosis of brain tumors often involves the use of Magnetic Resonance Imaging (MRI), with the Apparent Diffusion Coefficient (ADC) being a commonly employed technique in current clinical practice. This study seeks to investigate the potential of using statistical texture analysis of MRI-ADC images to distinguish between malignant and benign brain tumors.

Methods: The research utilized 980 MRI brain ADC image slices labeled as malignant and 805 labeled as benign from 252 subjects. The clinical diagnosis of each participant was verified by histopathological and radiological reports. The region of interest (ROI) was defined to extract ADC values within the tumor areas. From each ROI, statistical features including higher-order moments of ADC, mean pixel value, and texture features of Grey Level Co-occurrence Matrix (GLCM) were extracted along with patient demographic information. The mean feature values for each category were computed and analyzed using a one-tailed P value test at a 95% confidence level.

Results: The average pixel value of ADC, as well as the GLCM texture features (Variance 1, Variance 2, Mean 1, Mean 2, Contrast, and Energy), were found to be significantly higher ($P<0.05$) for benign tumors. In Contrast, malignant tumors exhibited significantly higher values for kurtosis of ADC and GLCM texture features (Entropy, Homogeneity, and Correlation). The patient's age and other features (skewness of ADC, GLCM texture features such as Shade, Entropy, and Prominence) did not provide sufficient evidence to reject the null hypothesis ($P>0.05$).

Conclusions: In conclusion, the aforementioned features, with the exception of the patient's age, skewness, and GLCM features such as Entropy, Shade, and Prominence can be used as potential biomarkers for distinguishing between benign and malignant brain tumors.

INTRODUCTION

Brain tumors are masses of abnormal tissue within the cerebrum that exhibit uncontrolled proliferation and evade the regulatory mechanisms that control normal cell division. This condition can arise in individuals of any age and is considered one of the prominent diseases affecting the central nervous system in humans [1]. Previous epidemiological studies indicate that the likelihood of developing a brain tumor at some point in their life is 29.9 per 100,000 individuals who are 20 years old or older in the United States. Among these brain tumors, approximately one-third are malignant, while the remainder is benign [2, 3]. Magnetic Resonance Imaging (MRI) is a commonly used and highly accurate medical imaging modality in current clinical practice for the diagnosis and therapeutic process of brain tumors. MRI scanner utilizes intense magnetic fields, magnetic field gradients, and radio frequency pulses to produce high-resolution images of internal body structures, including the soft tissues of the brain, such as gray matter, white matter, and cerebrospinal fluid [4, 5]. MRI is a non-invasive medical imaging technique that is based on the interaction between an applied magnetic field and the nuclear spin of atoms in the body. The MRI system applies gradient pulses and radiofrequency pulses to generate signals from the tissues being imaged. The signals are processed to create images with specific characteristics, known as MRI sequences. This article uses specific features of diffusion-weighted (DW) sequences of brain MRI images, besides others to distinguish benign brain tumors from malignant brain tumors.

Diffusion-weighted imaging (DWI) is a commonly employed MRI technique for identifying and classifying tumors in modern clinical practice [6]. The direction of water molecule diffusion or collective flow of water molecules in live tissues can be visualized using DWI, which is founded on the measurement of the random Brownian motion of water molecules within a voxel of tissue [7, 8]. The distinctive attribute of this tool has led to its widespread recognition as an essential instrument for studying the Central Nervous System (CNS). DW images are utilized to create Apparent Diffusion Coefficient (ADC) maps, which require the use of at least two types of images with varying diffusion sensitization levels (b-values). Typically, the lower limit is set to 0 s/mm2, while the upper limit ranges from 600 to 1000 s/mm2 [7, 9, 10]. However, there is evidence to suggest that ADC image generation can benefit from upper limits greater than 1000s/mm2 [11]. These images represent the extent of water molecule diffusion within live tissues and facilitate analysis of the image's texture features, which are characterized by repeated patterns or elements on its surface [12, 13]. The aim of texture analysis is to identify a distinct method of representing the underlying properties of textures, which can be expressed in a simplified and distinctive manner to describe the surface appearance of an image or object. The Grey Level Co-occurrence Matrix (GLCM) is a commonly used method for extracting statistical texture features that provide information about the spatial distribution of gray levels in grey-scale image textures, while also taking into account the spatial relationship between pixels [14-17]. Essentially, GLCM matrices quantify the frequency of one grey level's occurrence in relation to another specified grey level within a grey-scale image [18]. In this method, the relationship between grey intensities of adjacent pixels (a reference pixel and a neighboring pixel) in an image is analyzed to understand the variation in intensity at a specific pixel. GLCM matrices are generated by considering two parameters: the relative distance between the pixel pair and the angular relationship of the pixel pair. Typically, the orientation is classified into four angles: 0°, 45°, 90°, and 135°, and the average value of the resulting values in all four directions is used to extract the features (Equation 3) [18-21].

This study is subjected to applying GLCM statistical texture features, patients' demographics, second-order statistics, and higher-order moments of MRI brain tumor ADC images to distinguish between malignant and benign brain tumors by hypothesizing that there is a significant difference of means in extracted feature values between benign brain tumors and malignant brain tumors.

METHODS

The current study was a prospective analysis that

utilized 1785 MRI ADC image slices obtained from 252 subjects of both genders (with 52.97% male and 47.03% female participants) having been diagnosed with brain tumors through radiological methods and subsequently confirmed by histopathological evaluation (Figure 1).

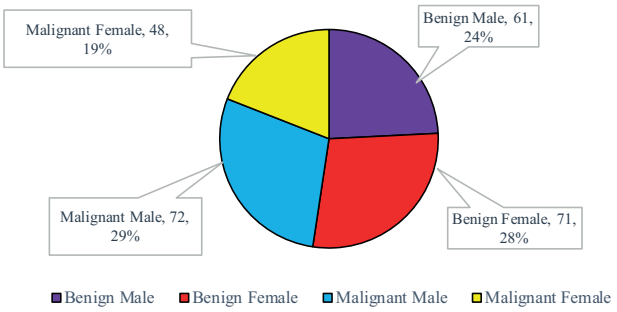

Figure 1: Gender Distribution Among Benign and Malignant Brain Tumor Categories

The study consisted of patients (n=252) diagnosed with malignant (n=120) and benign (n=132) brain tumors, covering an age range of 1 to 90 years. Patients undergoing chemotherapy or radiotherapy and those with incomplete patient information or poor-quality MRI images were excluded from the study. The Departments of Radiology and Histopathology at the National Hospital of Sri Lanka (NHSL) and Anuradhapura Teaching Hospital (ATH) provided MRI Digital Imaging and Communications in Medicine (DICOM) data, radiological and histopathological reports for this study. The data collection process took place over one year at both locations. Prior to conducting the study-related procedures, informed consent was obtained from patients. Ethical clearance certificate from both Ethics committees of NHSL and University of Peradeniya was also obtained. The malignant population mainly consisted of image slices from Glioblastomas multiforme (WHO IV), High grade gliomas (WHO III), Medulloblastomas (IV), and metastasis tumors, with percentages of 44.17%, 13.33%, 9.17%, and 18.33%, respectively. Pituitary Macro Adenomas (27.09%), Meningiomas (18.50%), and Schwannomas (16.77%) were the most common benign image slice population (Table 1 and Table 2).

Table 1: Tumors Types and the Composition of the Malignant Image Slice Population

	Patients, No.(%)	Slices, No.
Anaplastic Astrocytoma	2(1.67)	22
Anaplastic Meningioma	1(0.83)	11
Anaplastic Oligodendroglioma	3(2.50)	29
Central Astrocytoma	7(5.83)	65
Glioblastoma	53(44.17)	437
Hemorrhagic Metastasis	2(1.67)	23
High Grade Glioma (WHO III)	16(13.33)	147
Malignant Residuals	3(2.50)	22
Medulloblastoma	11(9.17)	108
Metastasis	22(18.33)	116

Table 2: Tumor Types and the Composition of Benign Tumor Population[a]

	Patients, No.(%)	Slices, No.
Astrocytoma	2(1.61)	13
Atypical Meningioma	1(1.24)	10
Choroid Meningioma	1(1.24)	10
Craniopharyngioma	2(1.37)	11
Dermoid Cyst CP Angle	1(1.61)	13
En Plaque Meningioma	3(3.60)	29
Ependymoma	1(0.87)	7
Frontal Cavernoma	1(0.50)	4
Meningioma	24(18.50)	149
Meningothelial Meningioma	2(3.72)	30
Pilocytic Astrocytoma	3(1.61)	13
Pituitary Macroadenoma	45(27.08)	218
Schwannoma	20(16.77)	135
Suprasellar Meningioma	2(0.87)	7
Diffuse Astrocytoma	1(0.74)	6
Glioma	4(3.60)	29
Hemangioblastoma	3(1.98)	16
Low Grade Glioma (WHO II)	10(8.94)	72
Oligodendroglioma	1(0.99)	8
Sphenoid Wing Meningioma	2(0.50)	4
Transitional Meningioma	3(2.61)	21

[a] Abbreviations: CP, Cerebellopontine; En, is derived from the French language and means “in”

All MRI scans were carried out using a 3T MR system and a head coil. The axial DW MRI data was acquired using the Echo-Planar Imaging (EPI) sequence with specific parameters such as a flip angle of 900, TE of 68ms and TR of 4300ms. The field of view (FOV) was set to 219mm×219mm with a matrix size of 124×124 and a slice thickness of 1mm. All ADC images were created by combining

the DICOM images of b=0 and b=1000 diffusion sensitization levels based on Equation 1.

Equation 1: $ADC = \sum_{i=1}^{n} \frac{\ln\left(S_i / S_0\right)}{b_I}$

The variables used in the equation are "i" for the image number, "Si" for the ith image, "S0" for the first image, "n" for the total number of images, and "bi" for the diffusion gradient value.

The image processing tasks and texture feature extraction activities were performed using a custom-built software named "Brain Lesion Differentiation and Identification Assistant" (BLeDIA), developed in Python 3.7. It included creating and visualizing ADC images, designing the region of interest (ROI) around the tumor area (Figure 2), generating GLCM matrices, and extracting features. To identify the tumor area, an ROI was drawn in the ADC images of each subject. Figure 2 depicts the ADC images of two malignant and two benign tumors with ROIs surrounding the tumors.

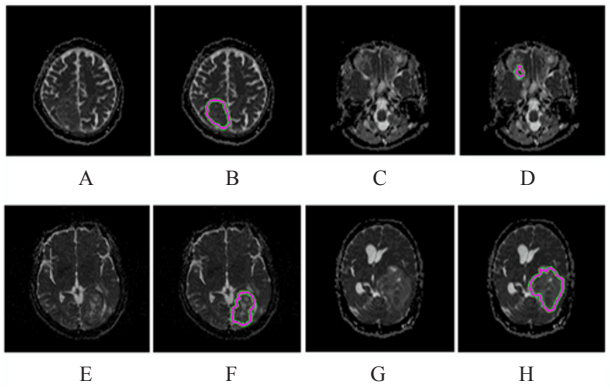

Figure 2: Four Different Types of Tumors and the ROI Drawn Surrounding The Tumor Area
A) ADC brain image of a 91-year-old male patient with meningioma condition (benign) in the right partial lobe; B) ROI selection of the image "A"; C) ADC brain image of a 59-year-old male patient with schwannoma (benign) condition in the right optic nerve; D) ROI selection of the image "C"; E) ADC brain image of a 55-year-old male patient with a high-grade glioma (WHO grade III) in the left parietal lobe; F) ROI selection of image "E"; G) ADC brain image of a 62-year-old male patient with a glioblastoma (WHO grade IV); H) ROI selection of image "G".

The average of the pixel-intensity values as well as the kurtosis and skewness values (Equation 2) were obtained from the ROIs selected for each ADC image. Following that, GLCM matrices (Equation 3) were generated for each ROI, and various statistical texture features such as GLCM Mean, Variance, Energy, Entropy, Contrast, Homogeneity, Correlation, Prominence, and Shade values were extracted from the generated GLCM matrices (Equation 4-12).

Equation 2: $n^{th}\ \text{moment} = \sum_i (p_i - p)^n . f(p_i)$

Whereas "pi" for the signal intensity in a specific pixel, "i" for the total number of pixels in the ROI, "p" for the average pixel value, and "f(pi)" for the probability of the signal intensity of that pixel.

The Grey Level Co-Occurrence Matrix

Equation 3:

$$L(x,y) = \begin{cases} \sum_{x,y=1}^{n} 1, if\ I(s,v) = x\ and\ I(s+\delta_{s,v}+\delta_v) = y \\ \sum_{x,y=1}^{n} 0, Otherwise \end{cases}$$

Whereas "I" represents 2D parametric ADC map with a matrix size of n x n, L(x,y) be the co-occurrence matrix that shows the probability of pixel pairs occurring together at specific spatial offsets between the pair, δs and δv, and with grey level values i and j.

Grey Level Co-Occurrence Matrix Mean

The left-sided equation is used to determine the mean value based on the reference pixel μi, while the right-sided equation is used to find the mean value based on the reference pixel μj. In the case of symmetrical GLCM matrices, both μi and μj are the same. However, if the matrices are not symmetrical, the two equations will yield different results.

‡**Equation 4:** $\mu_i = \sum_{i,j=0}^{N-1} i(P_{i,j})\ ;\ \mu_j = \sum_{i,j=0}^{N-1} j(P_{i,j})$

Grey Level Co-Occurrence Matrix Variance

GLCM Variance is a measure of the spread of the distribution about the mean, which is similar to other measures like Contrast or dissimilarity. The GLCM Variance specifically quantifies the extent to which

‡ P_(i,j) is co-occurrence matrix, N be the number of grey levels in the ADC image, μ for mean of P_(i,j), μ_i for mean of row i, μ_j is for the mean value of column j, σ_i represents the standard deviation of row i and σ_j represents the standard deviation of column j.

the neighbor and reference pixels in an image differ from each other by measuring the dispersion of the values around their mean.

‡**Equation 5:**

$$\sigma_i^2 = \sum_{i,j=0}^{N-1} P_{i,j(i-\mu_i)^2} \; ; \; \sigma_j^2 = \sum_{i,j=0}^{N-1} P_{i,j(j-\mu_i)^2}$$

Grey Level Co-Occurrence Matrix Energy

GLCM energy (ENR) quantifies the uniformity or Homogeneity of an image. It measures the sum of squared elements in the GLCM and reflects overall magnitude or strength of co-occurring pixel pairs. A higher Energy value indicates a more uniform or homogeneous texture, while a lower Energy value implies a more heterogeneous texture with varied gray-level distributions.

‡**Equation 6:** $ENR = \sum_{i,j=0}^{N=1} P_{i,j}^2$

Grey Level Co-Occurrence Matrix Entropy

GLCM entropy (ENT) is a statistical feature that characterizes the randomness or unpredictability of an image texture. It measures the amount of information or uncertainty in the distribution of co-occurring pixel pairs in the GLCM. A higher Entropy value indicates a more disordered or complex texture, while a lower Entropy value implies a more ordered or regular texture with fewer variations in gray-level distributions.

‡**Equation 7:** $ENT = \sum_{i,j=0}^{N-1} P_{i,j}(-\ln P_{i,j})$

Grey Level Co-Occurrence Matrix Contrast

GLCM contrast (CNT) quantifies the local variations or differences between adjacent pixel pairs in an image. It measures the intensity Contrast between pixels with different gray-level values in the GLCM and reflects the level of granularity or detail in an image. A higher Contrast value indicates a more distinct or sharp transition between neighboring pixel pairs, while a lower Contrast value implies a smoother or more gradual transition between pixel pairs.

‡**Equation 8:** $CNT = \sum_{i,j=0}^{N=1} P_{i,j(i-j)^2}$

Grey level co-occurrence matrix homogeneity

GLCM homogeneity (HOM) measures the closeness or similarity between neighboring pixel pairs in an image. It quantifies the inverse of the distance between pixels with different gray-level values in the GLCM and reflects the level of smoothness or uniformity in an image. A higher Homogeneity value indicates a more similar or homogeneous texture, while a lower homogeneity value implies a more heterogeneous texture with larger variations in grey-level distributions.

‡**Equation 9:** $HOM = \sum_{i,j=0}^{N-1} \frac{P_{i,j}}{1+(i-j)^2}$

Grey Level Co-Occurrence Matrix Correlation

GLCM correlation (COR) is a statistical feature quantifying the linear dependency or association between neighboring pixels in an image. It measures the similarity of the GLCM to a linear function and reflects the level of directionality or symmetry in an image texture. A higher correlation value indicates a stronger linear relationship between adjacent pixel pairs, while a lower correlation value implies a weaker linear relationship or a more complex texture with no clear directionality.

‡**Equation 10:** $COR = \sum_{i,j=0}^{N-1} P_{i,j} \left[\frac{(i-\mu_i)(j-\mu_j)}{\sqrt{(\sigma_i^2)(\sigma_j^2)}} \right]$

Grey Level Co-Occurrence Matrix Cluster Shade

GLCM cluster shade (CS) is a statistical feature that characterizes the skewness or asymmetry of the distribution of co-occurring pixel pairs in an image texture. It measures the deviation of the third-order moment of the GLCM from its expected value and reflects the level of clustering or groupings of pixel pairs in different directions or orientations.

‡**Equation 11:** $CS = \sum_{i,j=0}^{N-1} \{i + j - \mu_i - \mu_j\}^3 P_{i,j}$

Grey Level Co-Occurrence Matrix Cluster Prominence

GLCM cluster prominence (CP) is a statistical

‡ P_(i,j) is co-occurrence matrix, N be the number of grey levels in the ADC image, μ for mean of P_(i,j), μ_i for mean of row i, μ_j is for the mean value of column j, σ_i represents the standard deviation of row i and σ_j represents the standard deviation of column j.

feature that characterizes the sharpness or distinctness of the distribution of co-occurring pixel pairs in an image texture. It measures the deviation of the fourth-order moment of the GLCM from its expected value and reflects the level of clustering or groupings of pixel pairs in different directions or orientations. A higher cluster prominence value indicates a sharper or more distinct distribution with more pixel pairs clustered around the GLCM diagonal, while a lower cluster prominence value implies a flatter or less distinct distribution with fewer pixel pairs clustered around the diagonal.

‡Equation 12:

$$CS = \sum_{i,j=0}^{N-1} \{i + j - \mu_i - \mu_j\}^4 P_{i,j}$$

The values for GLCM mean and GLCM Variance can be calculated using either reference pixels μi or neighbor pixels μj, as per Equation 4 and Equation 5. For the symmetrical GLCM, where each pixel is counted once as a reference and once as a neighbor, both values should be identical. Finally, the mean values of each feature corresponding to malignant and benign brain tumor categories were measured. To determine the statistical significance of the difference in mean values between each tumor category for a particular feature, a two-sample P value test (one-tailed) was conducted with a 95% confidence level. In this study, the chi-square test was also applied to examine the potential relationship between the gender and the occurrence of benign and malignant brain tumors. The analysis intended to determine if there were any statistically significant differences in the incidence of these tumors between male and female individuals.

RESULTS

According to the results of the two-sample P value test (one-tailed), P values of the extracted features except for skewness of ADC (P>0.05) patient age (P>0.05) and GLCM texture features: Entropy (P>0.05), Shade (P>0.05), Prominence (P>0.05) showed significant differences in mean feature values between malignant and benign tumor categories. For benign tumors, the feature values for the mean pixel value of ADC (P<0.05) and six GLCM statistical texture features, GLCM Mean 1 (P<0.05), Mean 2 (P<0.05), Variance 1 (P<0.05), Variance 2 (P<0.05), Energy (P<0.05) and Contrast (P<0.05) showed significantly (P<0.05) higher values than malignant tumors. In Contrast, the mean feature values for Kurtosis of ADC (P<0.05), Homogeneity (P<0.05), and Correlation (P>0.05) showed significantly higher values for malignant tumors than benign tumors. However, the evidence provided by the P value for the skewness of ADC, patient's age, GLCM Entropy, GLCM Prominence, and GLCM Shade was not enough to prove whether there is a significant difference in mean feature values between malignant and benign tumor categories. The distribution pattern of values of each feature for malignant and benign tumor types is illustrated in Figure 3, and the distribution of feature values is showed in Figure 4 as boxplots. The findings of chi-square test indicate that male individuals are at a significantly higher risk of developing malignant brain tumors than female individuals (P<0.05). In Contrast, there was no significant association observed between gender and the occurrence of benign brain tumors (P>0.05) (Figure 1).

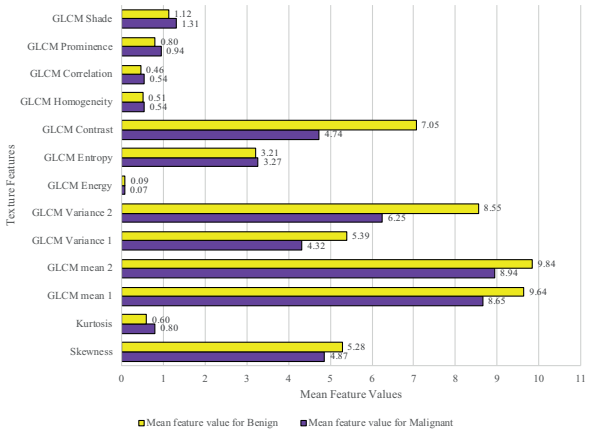

Figure 3: Distribution of Higher Order Moments of ADC, and GLCM statistical Texture Features Obtained for Benign and Malignant Brain Tumor Categories

DISCUSSION

The study was designed to identify key statistical texture features of MRI-ADC images that can be utilized as potential biomarkers in identifying and differentiating benign and malignant brain tumors.

‡ P_(i,j) is co-occurrence matrix, N be the number of grey levels in the ADC image, μ for mean of P_(i,j), μ_i for mean of row i, μ_j is for the mean value of column j, σ_i represents the standard deviation of row i and σ_j represents the standard deviation of column j.

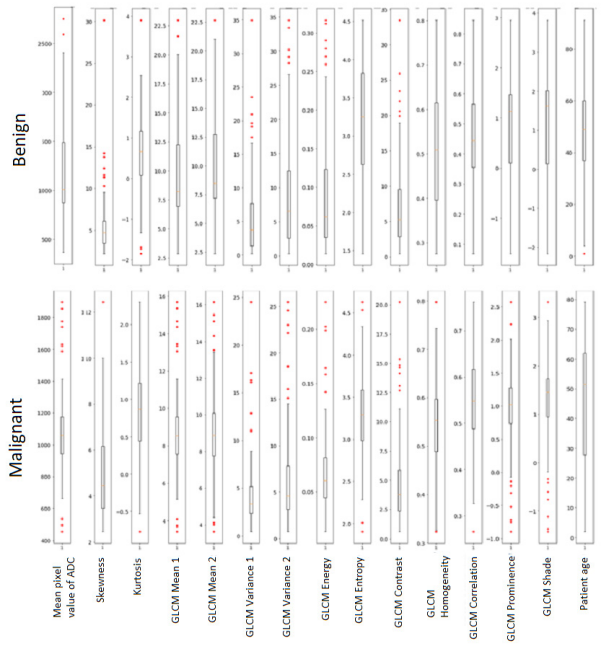

Figure 4: Distribution Pattern of the Texture Feature Values and Patient Age in Malignant and Benign Brain Tumors

The MRI DICOM (b=0 and b=1000 diffusion-weighted) images of brain tumor patients and the histopathological reports of selected subjects were collected retrospectively, after receiving both informed consents from each subject/bystander and the ethical clearance reports from the ethical review committees each institute collaborated in this study.

The data were collected over a period of one year, and at the end of the data collection process, the sample size reached up to 260 brain tumor subjects.

Participants without histopathological reports, corrupted MRI images, and subjects without proper identification details were excluded from the study. According to the above criteria, eight patients were excluded, and the study proceeded with 252 participants. However, the collected data revealed important epidemiological facts regarding the brain tumor population in Sri Lanka as a byproduct of this study. Based on the results, five out of fifteen features considered in this study (skewness of ADC, patient's age, GLCM Entropy, Shade, and Prominence) showed P values higher than 0.05, indicating that the mean values of these features for benign and malignant brain tumor categories are not significantly different. However, the study of GLCM texture features provides a comprehensive idea about the texture of both MRI-ADC images of benign and malignant brain tumors. The GLCM Energy results suggest that malignant tumors produce ADC images with higher uniformity than benign tumors (Equation 6), while GLCM Contrast indicates more

Table 3: Feature Values for Malignant and Benign Brain Tumor Categories [a]

	P Value[b]	Feature Value for Malignant (mean±SD)	Feature Value for Benign (mean±SD)
Mean Pixel Value of ADC	1.2660E-02	1071.5757±265.26	1184.0074±483.05
Skewness	1.0590E-01	4.8676±1.86	5.2809±3.14
Kurtosis	1.9840E-02	0.7996±0.61	0.599±0.88
GLCM Mean 1[c]	1.0430E-02	8.6452±2.26	9.6357±4.12
GLCM Mean 2[d]	1.4934E-02	8.937±2.29	9.8388±3.94
GLCM Variance 1[e]	3.7313E-02	4.3207±3.55	5.3887±5.56
GLCM Variance 2[f]	2.6164E-03	6.2539±4.85	8.5483±7.58
GLCM Energy	6.5663E-03	0.06874±0.03	0.087±0.07
GLCM Entropy	2.1528E-01	3.2748±0.48	3.2102±0.76
GLCM Contrast	1.1030E-04	4.738±3.46	7.0537±5.87
GLCM Homogeneity	2.6845E-02	0.5412±0.08	0.5128±0.13
GLCM Correlation	3.7513E-08	0.5434±0.09	0.4565±0.14
GLCM Prominence	9.9317E-02	0.9421±0.57	0.8047±1.02
GLCM Shade	1.0374E-01	1.3081±0.78	1.1242±1.40
Patient's Age	2.6122E-01	45.8416±21.48	47.3996±16.88

[a] Abbreviation: ADC, apparent diffusion coefficient; GLCM, grey level co-occurrence matrix

[b] $P<0.05$, statistically significant

[c] GLCM mean 1 represents GLCM mean value calculated based on the reference pixels µi

[d] GLCM mean 2 represents GLCM mean value calculated using the neighbor pixels µj

[e] GLCM Variance 1 represents GLCM Variance value calculated based on the reference pixels µi

[f] GLCM Variance 2 represents GLCM mean value calculated using the neighbor pixels µ

edges or wrinkled textures in ADC images of benign brain tumors than malignant brain tumors. GLCM Homogeneity describes a higher distribution of grey levels within the ADC images of malignant brain tumors compared to benign brain tumors. Lastly, GLCM Correlation reflects a significantly higher linear dependency of grey levels in ADC images of malignant brain tumors (Table 3, Figure 2).

The GLCM Mean and GLCM Variation provide details about the symmetry of the selected ROI of ADC brain tumor images and the dispersion of pixel values around the mean, respectively. However, in this study, we utilized them as GLCM Mean 1, GLCM Mean 2, GLCM Variance 1, and GLCM Variance 2 denoting the mean and Variance corresponding to ith and jth reference pixels in the GLCM matrix. When reviewing previous studies, it is evident that a significant amount of research has been conducted utilizing GLCM texture features, and histogram features (skewness and kurtosis) analysis of MR images to distinguish between benign and malignant carcinoma in various regions of the body such as the prostate, cervix brain, liver, etc. Moreover, some studies have employed GLCM texture analysis to assess the efficacy of cancer treatments. However, current literature does not offer substantial evidence to support the use of GLCM features of MRI-ADC in benign and malignant brain tumor classification. Andreas Wibmer et al., (2015) utilized GLCM texture features extracted from ADC and T1W MRI sequences of tumors to detect prostate cancers and differentiate Gleason scores (GS). The results of their study showed that prostate cancers located in the peripheral zone (PZ) have higher Entropy and Inertia and lower Energy, Correlation, and Homogeneity compared to non-cancerous tissue [22]. Korfiatis (2016) conducted a similar study to identify texture features that predict tumor differentiation and nodal status in diffusion-weighted imaging (DWI) of cervical carcinoma. However, this study utilized the grey-level matrixes and two histogram features (skewness and kurtosis) to achieve the task. In this study, the nodal status of the cervical carcinomas was correctly predicted by both the features skewness and kurtosis [23].

A study conducted by Vijithananda et al., (2019) on extracted histogram features (skewness and Kurtosis) from MRI-ADC images of brain tumors found similar results. They found that skewness and kurtosis provide useful information in distinguishing benign and malignant brain tumors [8]. A study by Wu et al., (2016) evaluated the use of GLCM texture features in combination with machine learning algorithms to differentiate between benign and malignant brain tumors using MRI T2-Weighted images. They found that GLCM features such as Contrast, Entropy, and Homogeneity were significant predictors for differentiating between benign and malignant tumors. The study concluded that texture analysis using GLCM features can be a useful tool for the non-invasive diagnosis and classification of brain tumors [24]. In another study, Kunimatsu et al., (2022) evaluated the use of GLCM texture features to differentiate between low-grade and high-grade gliomas using MRI images. They found that GLCM features such as Contrast, Homogeneity, and Energy were significantly different between low-grade and high-grade gliomas, with high-grade gliomas having higher values for these features [25]. Aggarwal in year 2022 conducted a study that explored the potential use of various spatial resolutions of GLCM texture features extracted from MRI images of brain tumors to create a tumor classification model using a random forest classifier. The texture features that were considered in the study included correlation, variance, entropy, inverse difference moment, dissimilarity, energy, contrast, and homogeneity. The study compared the classification accuracy for different values of steps and angles of GLCM, and the results indicated that reducing the spatial resolution of the image significantly reduced the method's performance. For example, using the same combination of offset and angles, the accuracy decreased from 83.3% to 61.1% when the spatial resolution was reduced from 64×64 to 32×32. The study confirmed that the spatial resolution used in this study (8-bit images (256×256 GLCM matrix)) is the optimum resolution to obtain the best GLCM feature values for the classification purposes [26]. The results of this study open up possibilities for future research in different directions such as developing machine learning models to classify benign and malignant brain tumors, differentiating between brain tumor types (e.g., meningioma, glioma, metastasis), and defining cut-off values for each feature. These avenues for further exploration may lead to more accurate and efficient diagnosis and treatment of brain tumors.

In conclusion, the evidence suggests that the value distribution pattern of GLCM texture features such

as Mean, Variance, Energy, Entropy, Contrast, Homogeneity, Correlation, Prominence, and Shade, as well as the kurtosis of ADC and the mean pixel values of ADC are correlated for both benign and malignant categories. Therefore, the study's outcomes suggest that utilizing aforementioned parameters can be used as potential biomarkers to identify and differentiate benign and malignant brain tumors. These results provide a confident conclusion for the utility of these parameters in diagnosing brain tumors.

ACKNOWLEDGMENTS

I would like to express my gratitude to the University of Peradeniya (Sri Lanka), University of Évora (Portugal), the ERASMUS Plus program, the National Hospital of Sri Lanka, Anuradhapura Teaching Hospital, and all the staff members, including consultants, in the radiology and histopathology departments of the aforementioned hospitals for their assistance, expertise, resources, and unwavering support, which were crucial in completing the study.

CONFLICT OF INTEREST

The authors declare that they have no conflicts of interest to report regarding the research presented in this article.

ETHICS APPROVAL

Ethical approvals for this study have obtained from two institutes

1. Ethical review board of the Faculty of Medicine, University of Peradeniya, Peradeniya, Sri Lanka. 2019/EC/50

2. Ethical review board of the National Hospital of Sri Lanka (NHSL), Colombo 10, Sri Lanka. ETH/COM/2019/AUGUST/05

REFERENCE

1. Jafarpour S, Sedghi Z, Amirani MC. A robust brain MRI classification with GLCM features. Int J Comput Appl. 2012;37(12):1-5.
2. Ostrom QT, Gittleman H, Truitt G, Boscia A, Kruchko C, Barnholtz-Sloan JS. CBTRUS Statistical Report: Primary Brain and Other Central Nervous System Tumors Diagnosed in the United States in 2011-2015. Neuro Oncol. 2018;20(suppl_4):iv1-iv86. DOI:10.1093/neuonc/noy131 PMID: 30445539.
3. Jemal A, Clegg LX, Ward E, Ries LA, Wu X, Jamison PM, et al. Annual report to the nation on the status of cancer, 1975-2001, with a special feature regarding survival. Cancer. 2004;101(1):3-27. DOI:10.1002/cncr.20288 PMID: 15221985.
4. Dadios EP. Fuzzy logic: algorithms, techniques and implementations: IntechOpen; 2012. 296 p. DOI:10.5772/2663.
5. Thamaraichelvi B, Yamuna G. Gray level co-occurrence matrix features based classification of tumor in medical images. ARPN J Eng Appl Sci. 2016;11(19):11403-14.
6. Maier SE, Sun Y, Mulkern RV. Diffusion imaging of brain tumors. NMR Biomed. 2010;23(7):849-64. DOI:https://doi.org/10.1002/nbm.1544.
7. Baliyan V, Das CJ, Sharma R, Gupta AK. Diffusion weighted imaging: Technique and applications. World J Radiol. 2016;8(9):785-98. DOI:10.4329/wjr.v8.i9.785 PMID: 27721941.
8. Vijithananda SM, Jayatilake ML, Weerakoon BS, Wathsala P, Thevapriya S, Thasanky S, et al., editors. Skewness and kurtosis of apparent diffusion coefficient in human brain lesions to distinguish benign and malignant using MRI. Recent Trends in Image Processing and Pattern Recognition: Second International Conference, RTIP2R 2018, Revised Selected Papers, Part II 2018 December 21–22; Solapur, India: Springer; 2019. DOI:10.1007/978-981-13-9184-2_17.
9. Sener RN. Diffusion MRI: apparent diffusion coefficient (ADC) values in the normal brain and a classification of brain disorders based on ADC values. Comput Med Imaging Graph. 2001;25(4):299-326. DOI:10.1016/s0895-6111(00)00083-5 PMID: 11356324.
10. Thormer G, Otto J, Reiss-Zimmermann M, Seiwerts M, Moche M, Garnov N, et al. Diagnostic value of ADC in patients with prostate cancer: influence of the choice of b values. Eur Radiol. 2012;22(8):1820-8. DOI:10.1007/s00330-012-2432-3 PMID: 22527373.
11. Kim CK, Park BK, Lee HM, Kwon GY. Value of diffusion-weighted imaging for the prediction of prostate cancer location at 3T using a phased-array coil: preliminary results. Invest Radiol. 2007;42(12):842-7. DOI:10.1097/RLI.0b013e3181461d21 PMID: 18007156.
12. Srinivasan GN, Shobha G, editors. Statistical Texture Analysis. Proceedings of world academy of science, engineering and technology; 2008.
13. Lerski RA, Straughan K, Schad LR, Boyce D, Bluml S, Zuna I. MR image texture analysis--an approach to tissue characterization. Magn Reson Imaging. 1993;11(6):873-87. DOI:10.1016/0730-725x(93)90205-r PMID: 8371643.
14. Sebastian V B, Unnikrishnan A, Balakrishnan K. Gray level co-occurrence matrices: generalisation and some new features. Int J Comput Sci Eng Inf Technol. 2012;2(2):151-7. DOI:10.5121/ijcseit.2012.2213.
15. Zulpe N, Pawar V. GLCM textural features for brain tumor classification. Int J Comput Sci Issue. 2012;9(3):354-9.
16. Pradeep N, Girisha H, Karibasappa K. Segmentation and feature extraction of tumors from digital mammograms. Comput Eng Intell Syst. 2012;3(4):37-46.
17. Pathak B, Barooah D. Texture analysis based on the gray-level co-occurrence matrix considering possible orientations. Int J Adv Res Electric Electron Instrum Eng. 2013;2(9):4206-12.
18. Baraldi A, Panniggiani F. An investigation of the textural characteristics associated with gray level cooccurrence ma-

trix statistical parameters. IEEE Trans Geosci Remote Sens. 1995;33(2):293-304.

19. Mokji MM, Bakar SA. Gray level co-occurrence matrix computation based on haar wavelet. Bangkok, Thailand: IEEE; 2007. DOI:10.1109/CGIV.2007.45.
20. Vijithananda SM, Jayatilake ML, Hewavithana B, Goncalves T, Rato LM, Weerakoon BS, et al. Feature extraction from MRI ADC images for brain tumor classification using machine learning techniques. Biomed Eng Online. 2022;21(1):52. DOI:10.1186/s12938-022-01022-6 PMID: 35915448.
21. Abbas Z, Rehman M-u, Najam S, Rizvi SD, editors. An efficient gray-level co-occurrence matrix (GLCM) based approach towards classification of skin lesion. Amity international conference on artificial intelligence (AICAI); 2019: IEEE.
22. Wibmer A, Hricak H, Gondo T, Matsumoto K, Veeraraghavan H, Fehr D, et al. Haralick texture analysis of prostate MRI: utility for differentiating non-cancerous prostate from prostate cancer and differentiating prostate cancers with different Gleason scores. Eur Radiol. 2015;25(10):2840-50. DOI:10.1007/s00330-015-3701-8 PMID: 25991476.
23. Korfiatis P, Kline TL, Coufalova L, Lachance DH, Parney IF, Carter RE, et al. MRI texture features as biomarkers to predict MGMT methylation status in glioblastomas. Med Phys. 2016;43(6):2835-44. DOI:10.1118/1.4948668 PMID: 27277032.
24. Wu S, Zheng J, Li Y, Wu Z, Shi S, Huang M, et al. Development and Validation of an MRI-Based Radiomics Signature for the Preoperative Prediction of Lymph Node Metastasis in Bladder Cancer. EBioMedicine. 2018;34:76-84. DOI:10.1016/j.ebiom.2018.07.029 PMID: 30078735.
25. Kunimatsu A, Yasaka K, Akai H, Sugawara H, Kunimatsu N, Abe O. Texture Analysis in Brain Tumor MR Imaging. Magn Reson Med Sci. 2022;21(1):95-109. DOI:10.2463/mrms.rev.2020-0159 PMID: 33692222.
26. Aggarwal AK. Learning texture features from GLCM for classification of brain tumor mri images using random forest classifier. Trans Signal Process. 2022;18:60-3. DOI:10.37394/232014.2022.18.8.